
Solving Inverse Problems in Stochastic Self-organizing Systems through Invariant Representations

Elias Najarro[‡]

 0000-0002-7875-3251
IT University of Copenhagen
2300 Copenhagen, Denmark

Nicolas Bessone[‡]

 0009-0008-9008-0003
IT University of Copenhagen
2300 Copenhagen, Denmark

Sebastian Risi

 0000-0003-3607-8400
IT University of Copenhagen
2300 Copenhagen, Denmark

Abstract

Self-organizing systems demonstrate how simple local rules can generate complex stochastic patterns. Many natural systems rely on such dynamics, making self-organization central to understanding natural complexity. A fundamental challenge in modeling such systems is solving the inverse problem: finding the unknown causal parameters from macroscopic observations. This task becomes particularly difficult when observations have a strong stochastic component, yielding diverse yet equivalent patterns. Traditional inverse methods fail in this setting, as pixel-wise metrics cannot capture feature similarities between variable outcomes. In this work, we introduce a novel inverse modeling method specifically designed to handle stochasticity in the observable space, leveraging the capacity of visual embeddings to produce robust representations that capture perceptual invariances. By mapping the pattern representations onto an invariant embedding space, we can effectively recover unknown causal parameters without the need for handcrafted objective functions or heuristics. We evaluate the method on three self-organizing systems: a physical, a biological, and a social one; namely, a reaction-diffusion system, a model of embryonic development, and an agent-based model of social segregation. We show that the method reliably recovers parameters despite stochasticity in the pattern outcomes. We further apply the method to real biological patterns, highlighting its potential as a tool for both theorists and experimentalists to investigate the dynamics underlying complex stochastic pattern formation.

1 Introduction

Complex systems—such as cellular automata, reaction-diffusion, or agent-based models (ABM)—self-organise into complex dynamical patterns driven by simple rules. The conventional modeling approach of complex systems consists of making an educated guess of the local rules, simulating them—be it a partial differential equation, a cellular automaton, or an agent-based model—and observing whether the emergent patterns are compatible with the phenomena we seek to explain. This modeling approach has proven highly successful in providing mechanistic understanding of a variety of phenomena, including early work on social segregation in urban environments [1], sociology [2], financial markets dynamics [3], and ecology [4, 5]. For instance, in the context of morphogenesis [6, 7], Manukyan et al. [8] identified the specific cellular automata rule and the underlying reaction-diffusion process that give rise to the skin patterns present in ocellated lizards.

[‡]Equal contribution.

Inverse modeling formulates the problem in the reverse causal direction: “Given these macroscopic observations, what are the underlying rules that produce them?” [9, 10]. An inverse model takes an observation as input and returns the model, or initial configuration, that generates the observation. See Fig. 1 for a visual summary of inverse modeling and some of its difficulties.

A major challenge in inverse problems is the presence of stochasticity in the observations. Natural phenomena, notably those associated with complex systems, exhibit sensitivity to initial conditions. That is, the same model, under slightly different initial conditions, evolves towards divergent patterns [11–13]. Often, these patterns share high-level features but do not match when compared pixel by pixel. They are stochastic instances of the same class of patterns—see Fig. 2 for an example of stochastic patterns in self-organizing systems. For instance, while every human fingerprint is unique, they all share characteristic features that make them recognisable as fingerprints. Similarly, no two leopards have identical spot motifs, yet all are immediately identifiable as leopard patterns. In mathematical terms, patterns can belong to the same class in the presence of invariances—be it translational, rotational, or of another kind.

In this work, we introduce a method that addresses the challenge of solving inverse problems in systems with stochastic observable patterns. The method operates by mapping target patterns onto an invariant embedding representation, enabling efficient recovery of inverse parameters in stochastic self-organizing systems without the need for heuristics or hand-crafted loss functions.

Contributions ① *Conceptually*, we introduce a method to efficiently solve inverse problems in stochastic self-organizing systems by leveraging visual embedding models to generate invariant representations of observable patterns. ② *Technically*, we develop an optimization framework that combines evolutionary strategies with pre-trained embedding models to address stochasticity in the observable space in inverse problems. ③ *Empirically*, we evaluate our method on three distinct—physical, biological, and social—self-organizing systems: Gray-Scott’s reaction-diffusion model, a model of early embryonic development in mammals, and an agent-based model of social segregation. Results show that geometric invariances can be effectively captured, thereby overcoming the challenges posed by pattern stochasticity in the observable space.

2 Background

Self-organizing systems Self-organization, understood as the spontaneous emergence of global order or coordination in a system from local interactions of its parts, is observed across different physical, biological, and social systems [14–16]. Examples range from morphogenesis, where cells divide and specialise to form complex body plans in living organisms [17, 18], to animal skin patterns Murray [12] or flocking birds [19]. In social systems, this phenomenon is demonstrated in ABMs, such as Schelling’s segregation model, where simple local rules lead to emergent segregation patterns akin to those observed in cities [1].

Self-organizing systems are highly sensitive to initial conditions. This sensitivity results in stochastic emergent patterns. For example, the formation of fingerprints or animal skin patterns is driven by genetic signals, local cellular feedback, and mechanical constraints that result in unique patterns on each individual. Even slight variations in initial conditions can produce vastly different results. This property of complex systems poses a significant challenge to inverse problem-solving methods: it requires defining a loss metric that captures the equivalence of patterns with inherent variability.

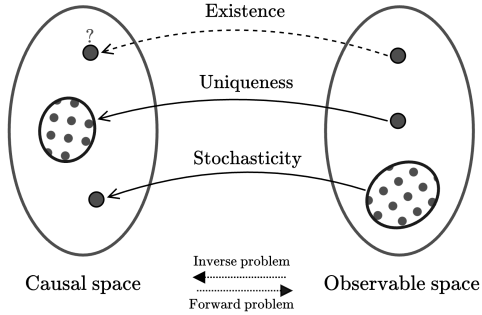
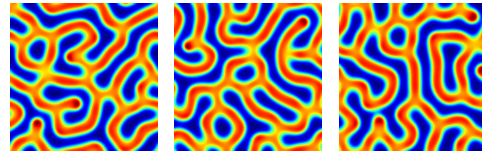


Figure 1: **Inverse problem diagram.** Inverse modeling consists in finding the mapping from observations to their causal space (also referred to as *parameter space*, *solution space* or *domain space* in the literature). It presents several challenges: (i) solutions may not exist for all observations; (ii) the problem of uniqueness: multiple causes may produce identical observations; and (iii) observations may be stochastic, resulting in different observed patterns for the same model parameters. Our method seeks to address the challenge of stochasticity in the observable space.

Inverse problems Solving an *inverse problem* consists in determining the unknown parameters, or initial conditions, of a system from observations of its outcomes [9]. By contrast, *forward problems* unambiguously map inputs to outputs using the system model. Formally, solving an inverse problem requires finding $(\theta, s_0) \in \Theta \times S$ such that $F(\theta, s_0) = y_{\text{obs}}$, where $F : \Theta \times S \rightarrow Y$ denotes the forward model mapping parameters $\theta \in \Theta$ and initial states $s_0 \in S$ to observed data $y_{\text{obs}} \in Y$. Inverse problems are typically ill-posed, characterised by solution sensitivity and non-uniqueness [20]. These properties link inverse problems to complex systems: small changes in their parameters or initial state can result in divergent outcomes. As such, recovering the causal parameters—i.e., solving the inverse problem—shares similar challenges with ill-posed problems.

Stochasticity can be present in inverse problems in two distinct ways. **Stochasticity in the causal space:** multiple parameters or initial conditions $(\theta, s_0) \in \Theta \times S$ map to identical or nearly identical observations $y_{\text{obs}} \in Y$, resulting in degenerate solutions and non-uniqueness, i.e., non-injectivity of F . In this case, the unknown quantities in the causal space are distributions. An example is seismic tomography, which uses seismic waves recorded at the surface to reconstruct the Earth’s interior. Solutions are non-unique: similar surface measurements can originate from different inner structures. **Stochasticity in the observable space:** in this case, observations are inherently stochastic. Either resulting from randomness in initial states, such as in reaction-diffusion systems ($y_{\text{obs}} = F(\theta, s_0)$ with $s_0 \sim S$), or from intrinsic stochasticity in the forward model F , as in the asynchronous updates of an agent-based model. See Fig. 2. The existing literature on *inverse stochastic modeling* exclusively focuses on the first case: how to address stochasticity in the causal space [21–26], where similar observations can have different causal origins. By contrast, the method proposed in this work addresses the challenge of stochasticity in the observable space.

Gray-Scott - $D_u = 1.0, D_v = 0.5, f = 0.055, k = 0.062$



Schelling’s model of segregation - Tolerance = 0.7



Figure 2: Stochasticity in self-organizing systems. Three simulation instances of two self-organizing models run with the same parameters. (*Top*): Reaction-diffusion model; the stochasticity results from varying initial conditions $s_0 \sim S$. (*Bottom*): Schelling’s model segregation; the stochasticity is present in the model F itself in the form of asynchronous updates. Both systems are examples of stochasticity in the observable space.

Embedding Representations Visual embeddings are learned vector representations that capture relevant features of images beyond the raw pixel values. Instead of encoding only low-level information, such as colour and intensity, embeddings represent higher-level visual attributes, such as shape, texture, structure, and semantic content [27–31]. Visual embedding models transform image data into a lower-dimensional space where semantically or visually similar images are mapped to nearby points, while dissimilar images are placed farther apart [32–34]. See diagram in Fig. 3a.

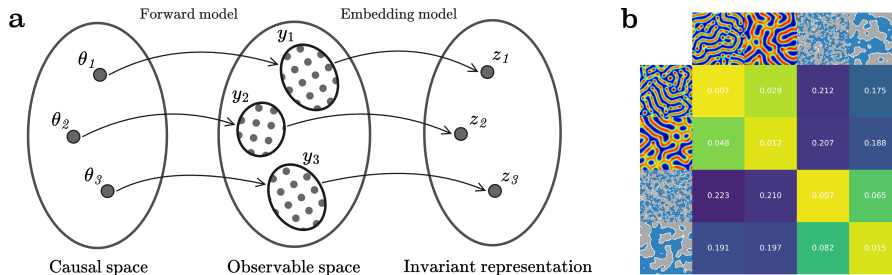


Figure 3: Invariant representations. (a): Diagram representing models parameters θ_i , generating observable patterns y_i , and the visual patterns being mapped to an embedding z_i . (b): Distance matrix between embedding representations z of four patterns (two reaction-diffusion and two ABM segregation patterns). Notice that each of the patterns is a unique instantiation of the model. Similarity clusters appear, suggesting that the embedding model represents patterns with similar features as similar vectors. The values displayed are pairwise cosine distances $1 - \cos(z_i, z_j)$.

Geometric invariant representations. Embedding representations have been shown to be invariant under different pattern transformations [35–39]. For instance, Moskvayak and Maire [32] showed that convolutional embeddings can produce invariant representations of animal patterning under homographic transformations. We demonstrate our method with CLIP [33], an open-source vision and text embedding model trained on large-scale datasets using contrastive learning (in this work, only the visual encoder is used). Its embeddings, represented as 512-dimensional vectors, capture high-level visual features. The large variety of images seen by CLIP during training results in rich representations, making them suitable for general-purpose applications without requiring additional fine-tuning. Fig. 3b shows that CLIP embeddings are able to capture relevant visual features.

3 Proposed Method

A common approach to solving inverse problems is to formulate them as optimization problems by defining a loss function that measures the discrepancy between target data and predictions [21, 22]. However, pixel-based metrics are unable to meaningfully capture feature similarities between stochastic patterns. Therefore, they cannot account for the intrinsic variations often present in self-organizing patterns. To solve inverse problems with stochasticity in the observable space, a metric capable of capturing the feature-level similarities rather than exact pixel-level matches is needed. Embedding representations offer an effective solution to this challenge by encoding features and invariances of the patterns. The idea behind the proposed method is straightforward: map stochastic patterns onto an embedding space where perceptually similar patterns have similar vector representations. Then, use these invariant representations to solve the inverse problem of finding the unknown parameters that generate the stochastic patterns we seek to reconstruct. A visual summary is provided in Fig. 4.

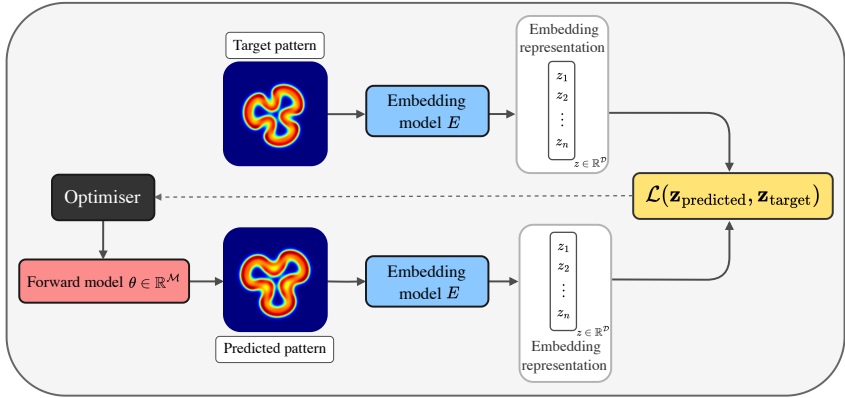


Figure 4: **Method overview.** A target pattern is mapped onto an embedding space $z_{\text{target}} \in \mathbb{R}^D$ using the embedding model E , where D is the embedding space dimension. A forward model, parametrised by $\theta \in \mathbb{R}^M$, where M is the degrees of freedom of the model, generates a pattern which is mapped to the same embedding space resulting in z_{solution} . The loss \mathcal{L} between the target and the candidate solution embedding guides the optimizer, iteratively updating θ until convergence. By operating in embedding space, the method offers robustness against the inherent stochasticity of emergent patterns.

We demonstrate the method using CLIP, a pre-trained embedding model, to encode the visual patterns into vector embeddings z . Both the target and the predicted patterns are mapped onto the same embedding space, resulting in similar representations despite stochastic variations. A black-box optimizer is then used to search for the inverse parameters that minimise the embedding distance between the target pattern and the predictions.

We use CMA-ES (Covariance Matrix Adaptation Evolution Strategy), a population-based optimizer [40], to search the causal space. Evolutionary strategies have been shown to find high-performing solutions in a variety of tasks [41–43]—including in the context of inverse problems [44, 45]. CMA-ES operates by iteratively updating the covariance matrix of a multivariate normal distribution at each generation, so that candidate solutions θ_i are increasingly guided towards promising regions of the

search space. Solutions are iteratively sampled from a Gaussian distribution centred on the current mean with the covariance defining the search distribution: $\theta_i = \mathbf{m} + \Delta \mathbf{C}^{1/2} \sigma$ with $\sigma \sim \mathcal{N}(\mathbf{0}, \mathbf{I})$ where \mathbf{m} is the mean, Δ is the step-size, \mathbf{C} is the covariance matrix and \mathbf{I} is the identity matrix. The mean \mathbf{m} is updated as a weighted sum of selected solutions $\mathbf{m}_{\text{new}} = \sum_{k=1}^{\mu} w_k \theta_k$ where μ is the number of selected solutions, and w_k are the weights based on solution rank.

The method operates as follows: **(1)** sample a set of parameters θ_i and random initial states $s_0 \sim \mathcal{S}$, **(2)** generate the corresponding patterns y_i through the forward model F , **(3)** use the embedding model to encode the resulting patterns into the embedding space z , **(4)** compute the loss between the target z_{target} and the candidate solutions’ embeddings z_{solution} , and **(5)** update the optimizer accordingly. In the case of CLIP, the loss metric is cosine similarity. By focusing on high-level visual similarities rather than pixel-level matches, the method is robust to stochastic variations, and is able to solve inverse problems across entire families of patterns with shared visual features—without requiring handcrafted loss functions. The method is detailed in Algorithm 1.

Algorithm 1 Inverse modeling through embedding representation

Require: Forward model F , State space S , Loss function \mathcal{L} , Embedding model E , optimizer

- 1: Choose target pattern y_{target}
 - 2: **while** not converged **do**
 - 3: Sample candidate solutions θ_i from optimizer
 - 4: Sample an initial configuration $s_0 \in S$
 - 5: Run simulations: $y_{\text{solution}} \leftarrow F(\theta_i, s_0)$
 - 6: Map patterns to embedding space:
 - 7: $z_{\text{target}} \leftarrow E(y_{\text{target}})$
 - 8: $z_{\text{solution}} \leftarrow E(y_{\text{solution}})$
 - 9: Compute loss: $loss_i \leftarrow \mathcal{L}(z_{\text{solution}}, z_{\text{target}})$
 - 10: Update optimizer state with $loss_i$
 - 11: **end while**
 - 12: **return** $\theta = \arg \min_{\theta} loss_i$
-

4 Experiments and Results

In this section, we present the results of applying the method to three self-organizing systems: a reaction-diffusion system known as the Gray-Scott model [46, 47], a model of embryonic development [48], and Schelling’s agent-based model of segregation [1]. We chose these three distinct systems, both in terms of scientific domain (physics, biology and sociology) and the underlying mathematical model (PDE vs. ABM), to highlight the generality of the method. We first introduce the models, then formulate them as inverse problems, and subsequently present the results of applying the method. Finally, we evaluate the method on two non-simulated patterns: an ocellated lizard and a zebra skin pattern.

Hardware details. Experiments have been run on a single machine with a *AMD Ryzen Threadripper 3990X* CPU and a *NVIDIA GeForce RTX 4090* GPU. **Reproducibility.** The codebase including the algorithm implementation and scripts used to run the reported experiments can be found in <https://github.com/enajx/InverseStochastic>.

4.1 Physical system: Reaction-Diffusion system

Gray-Scott is a reaction-diffusion model used to study pattern formation in developmental systems [46, 47]. It describes how spatially distributed concentrations of two interacting substances—or morphogens—evolve over time. Morphogens play a critical role in developmental biology by guiding cell differentiation and tissue patterning through their concentration gradients. u represents a nutrient or precursor substance, while v acts as an autocatalyst that promotes its own production while consuming u . The interaction between u and v , combined with their ability to diffuse through space, leads to the emergence of complex patterns such as spots, stripes, or labyrinths. Through this interplay, the Gray-Scott model provides insights into how local reactions and diffusion contribute to the self-organization of biological structures. It is formalised as two partial differential equations:

$$\begin{aligned} \frac{\partial u}{\partial t} &= D_u \nabla^2 u - uv^2 + f(1 - u) \\ \frac{\partial v}{\partial t} &= D_v \nabla^2 v + uv^2 - (f + k)v \end{aligned}$$

- u and v are the chemical concentrations.
- D_u and D_v are the diffusion rates for u and v .
- f is the feed rate of u .
- k is the kill rate of v .
- ∇^2 is the Laplacian representing diffusion.

By convention, the u field is treated as a latent variable, while the v field represents the morphogens interpreted as visible patterns.

4.1.1 Results Reaction-Diffusion

In order to find the unknown parameters for the reaction-diffusion system, we follow the algorithm described in Algorithm 1. At each optimization run, we first generate a target pattern for a set of parameters $\{D_u, D_v, k, f\}_{target} \in \mathbb{R}^4$ by simulating Gray-Scott partial differential equations 4.1 from a random initial state $s_0 \sim \mathcal{S}$ for 1000 steps. The resulting pattern is embedded onto z_{target} with the vision model CLIP. z_{target} serves as the target embedding for the loss throughout the optimization process. Then, the optimizer samples a population of candidate solutions, $\{D_u, D_v, k, f\}_i \in \mathbb{R}^4$, used to simulate the dynamics of reaction-diffusion. The generated patterns y_i are then passed through the embedding model, resulting in z_i . We compare each z_i against the target embedding z_{target} using cosine similarity $\cos(z_i, z_{target})$. The optimization is iteratively run until it converges to a solution that maximizes the cosine similarity with respect to the target embedding z_{target} . Results for three sets of reaction-diffusion parameters and their corresponding training curves are shown in Fig. 5.

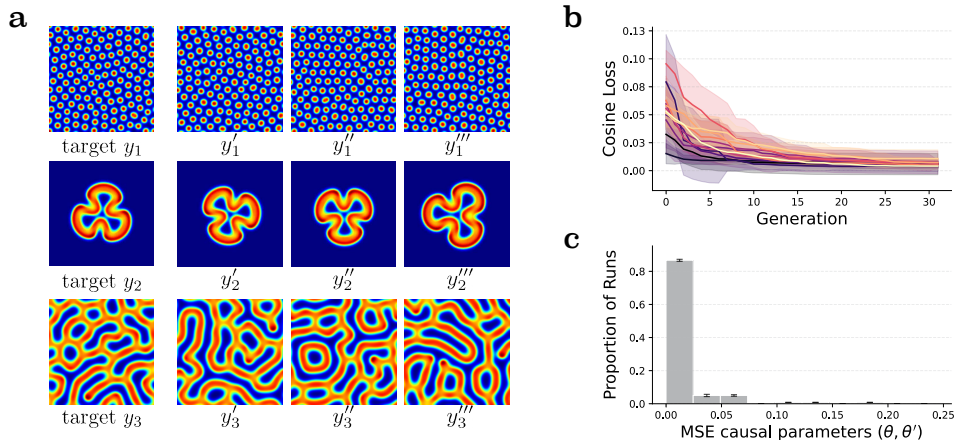


Figure 5: **Results for Gray-Scott reaction-diffusion system.** (a): A selection of three target patterns y_i (left column), and three reconstructions y'_i, y''_i, y'''_i of the causal parameters found by the inverse method on three independent training runs. The method reconstructs patterns with features that qualitatively match the targets. (b): Loss curves showing the average loss and variance of 10 training runs for 12 different patterns. (c): Histogram showing the mean-square errors between the causal θ and optimized parameters θ' ; error bars indicate one standard deviation of the 10 training runs averaged for all the 12 target patterns.

Results for 10 independent training runs on a set of 12 target patterns are shown in Fig. 11. The loss curves and histogram in Fig. 5 reflect results for the full set of twelve target patterns. Fig. 14 shows the cosine distance matrix between CLIP embeddings of the set of target patterns used.

4.2 Biological system: Embryonic development

A blastocyst is the early-stage of the mammalian embryo. It is composed of three main components, an outer cellular layer, the trophoblast, which later in development becomes the placenta, and an inner cellular cluster, the embryoblast that develops into the organism itself, and a layer, the hypoblast, separating the embryoblast from the internal cavity; the cellular arrangement of the embryo at the blastocyst stage is shown in Fig. 6a. Due to the stochastic nature of morphogenesis, the exact position where the stem cells differentiate the embryoblast varies with each developmental instance.

The blastocyst simulation is based on Cang et al. [48] Cellular Potts Model (CPM), where the gene regulatory network model defined as a set of stochastic differential equations guide the cells’ differentiation. Unlike in the reaction-diffusion experiments, the blastocyst has a single stochastic target pattern, representing the observed embryogenic developmental process in mammalian organisms [48, 49]. The simulation is performed using Morpheus library and based on Morpheus [50]’s implementation.

4.2.1 Results - Embryonic development

In accordance with the embryonic development literature [48], a successful developmental process is one that leads to a cellular arrangement where the inner cell mass, or embryoblast, adheres to the outer layer, or trophoblast, while having a thin endodermic layer, or hypoblast, facing towards the inner cavity. An instance of this developmental pattern is shown in Fig. 6a. The inverse problem consists in finding a set of four Hill coefficients that modulate the expression of several transcription factors and proteins, acting as a complex genetic switch that guides development. Next to the target pattern, Fig. 6a shows the outcome of three independent optimization runs that correctly recover the parameters resulting in successful developmental patterns. For ten independent optimization runs, using CLIP embedding model to guide the optimization results in seven successful pattern recoveries—by contrast, using MSE as the optimization metric, results in only one correct developmental patterning. Results of embedding model and baseline metrics are shown in Table 1, and the obtained patterns for ten optimization runs are shown in Fig. 12.

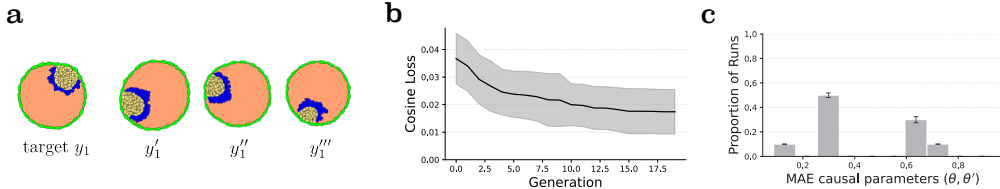


Figure 6: **Results for blastocyst model.** (a): Target pattern and found solutions from three independent runs to recover the blastocyst parameters. (b): Training curve showing the average loss and variance for the target pattern over ten optimization runs. (c): Histogram showing the mean-square errors between the causal θ and optimized parameters θ' ; error bars indicate one standard deviation of the 10 training runs for each tolerance target.

4.3 Social system: Schelling’s Model of Segregation

The third system we use to demonstrate the method is Schelling’s segregation model [1], a classic computational model used to study spatial pattern emergence in social systems. It illustrates how individual preferences for neighbourhood composition can lead to large-scale segregation. Schelling’s model has been highly influential in computational social science, contributing to the understanding of segregation and its implications for urban planning and social dynamics. Schelling’s model has historical significance in computational social science, as it was one of the first to show how simple local rules can produce complex emergent behaviours, highlighting the potential of agent-based models for social systems [16, 51]. For this latter reason, we chose it to demonstrate our method.

Our implementation consists of two classes of agents, randomly distributed on a spatial grid. Each agent evaluates its satisfaction based on the proportion of similar neighbours in its local neighbourhood. Unsatisfied agents with their current location will asynchronously relocate to a random location to improve their satisfaction. Schelling’s model leads to the emergence of complex segregation patterns that match those observed in urban environments.

$$S_i = \begin{cases} 1 & \text{if } \frac{N_{\text{similar}}}{N_{\text{total}}} \geq T \\ 0 & \text{otherwise} \end{cases}$$

- S_i is the satisfaction of agent i .
- N_{similar} is the number of similar neighbours.
- N_{total} is the total number of neighbours.
- T is the agent’s tolerance threshold, $T \in [0, 1]$.

The emergent patterns, while differing at the microscopic level, exhibit consistent macroscopic structures and statistical properties. It is these invariances of the macroscopic patterns that our method exploits to find the unknown threshold.

4.3.1 Results - Schelling Segregation Model

In this experiment, the same optimization methodology described in Algorithm 1 is applied to find the tolerance T from different Schelling segregation patterns. We use a grid size of 100 by 100, and an occupation density of 90%. The results of the experiment are presented in Figure 7.

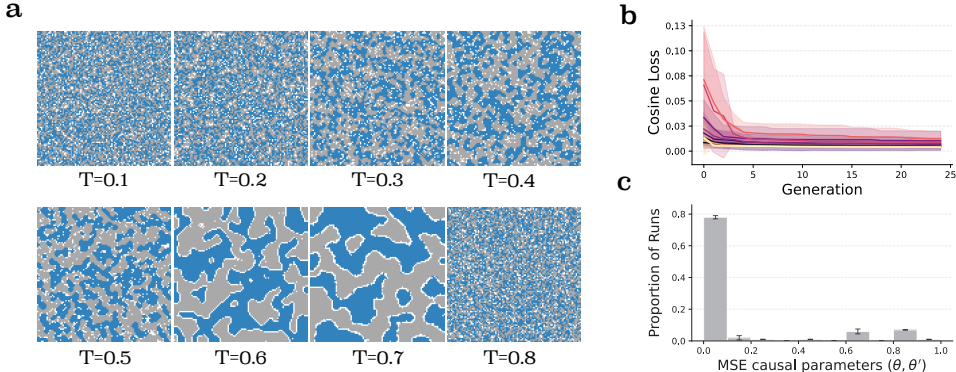


Figure 7: **Results for Schelling segregation model.** (a): Schelling runs with *tolerance* parameter $T \in \{0.1i \mid i \in \{1, 2, \dots, 8\}\}$. For small values of T , agents converge with minimal migration as tolerance threshold is quickly satisfied, in middle range of T (3-6) segregation patterns become more pronounced, while for large values of T the system does not converge as threshold is unattainable. (b): Training curve showing the average loss and variance for target patterns associated with each system’s tolerance. (c): Histogram of mean-square errors between the causal θ and optimized parameters θ' .

The method successfully finds the inverse parameters. The curves and histogram of Fig. 7 indicate the mean and standard deviation of 10 independent training runs. The patterns resulting from each training run are shown in the appendix Fig. 13.

4.4 Baselines comparison

Table 1: Loss values (median \pm MAD across ten runs) for ten runs per target pattern under two embedding metrics (CLIP, Nomic), Fréchet Wavelet and the domain-specific metrics. Results ranked by z-score across metrics.

	Reaction-Diffusion	Blastocyst	Schelling	z-score
CLIP	0.038 \pm 0.021	0.321 \pm 0.097	0.044 \pm 0.033	-1.08
Fréchet Wavelet	0.050 \pm 0.032	0.333 \pm 0.087	0.040 \pm 0.031	-0.99
Nomic	0.042 \pm 0.022	0.408 \pm 0.028	0.054 \pm 0.041	-0.75
Dissimilarity index	0.222 \pm 0.060	0.483 \pm 0.107	0.040 \pm 0.028	0.39
Edge density	0.111 \pm 0.045	0.517 \pm 0.198	0.265 \pm 0.226	0.61
MSE	0.158 \pm 0.082	0.507 \pm 0.099	0.200 \pm 0.129	0.63
Orientation variance	0.126 \pm 0.072	0.639 \pm 0.119	0.299 \pm 0.239	1.19

We compare the performance of the embedding representations against six other baselines: mean squared error (MSE) for pixel-level comparison, Nomic, a second embedding model [52]; Fréchet Wavelet, a metric based on wavelet packet decomposition [53]; and a set domain-specific metrics: dissimilarity index, which measures spatial clustering patterns in agent-based models; edge density, quantifying boundary structures; and orientation variance, capturing directional pattern features. Results show that CLIP achieves the lowest z-score (-1.08), demonstrating the best overall performance across systems. While dissimilarity index performs optimally for its specific domain (i.e., segregation cluster), it performs poorly when evaluated in other patterns (z-score: 0.39). Other domain-specific metrics such as edge density and orientation variance show substantially worse overall performance (z-scores: 0.61 and 1.19 respectively). MSE ranks second to last (z-score: 0.63)—expectedly, pixel-to-pixel distance does not provide a good error signal to guide the optimization. The experiments results are shown in Table 1; variability is reported using median absolute deviation (MAD) given non-normal error distributions. Results demonstrate the effectiveness of invariant embeddings for handling stochasticity in the observable space without requiring domain-specific loss metrics.

4.5 Natural patterns

In this section, we evaluate the method on natural patterns—rather than simulated ones, as in the previous experiments. First, on the skin patterning from an ocellated lizard. We provide the method with a target image obtained from Manukyan et al. [8] and search for the unknown parameters of a Gray-Scott reaction-diffusion model to reconstruct the patterns following the same methodology described in 1. The target image and the reconstructed one are shown in Fig. 8.

Guiding Model Testing Identifying unknown parameters underlying natural patterns is a significantly more challenging problem as there is no guarantee that the chosen model can generate the target patterns. We often lack an exact model of the underlying process. In such cases, one can approach the problem by including the functional form of the model itself and have the optimizer predict the model’s functional form and parameters—an optimization technique known as symbolic regression [54]. However, the space of possible models is extremely large, and furthermore, we often have an intuition about the model. In such cases, we can conjecture a minimal model form that might be driving the process that generates the target pattern. We can then apply the inverse method to tune the free parameters of the model to reconstruct the natural target. If the model’s expressivity is insufficient to capture the pattern, we can iteratively complexify the model. This approach allows us to preserve a mechanistic understanding of the underlying process until the model captures the target pattern.

In this second experiment with natural patterns, we aim at finding the reaction-diffusion parameters that lead to a zebra skin pattern [55]. In our initial attempt at generating a zebra-like pattern, we found that the standard Gray-Scott reaction-diffusion model failed to produce matching results. This suggests that the underlying mechanism responsible for the zebra pattern differs from the assumed model. The Gray-Scott model is isotropic, meaning it treats diffusion equally in all directions, which makes it challenging to generate stripe patterns. To overcome this limitation, we introduced anisotropy into the partial differential equations by allowing the diffusion coefficients to vary directionally:

$$\begin{aligned} \frac{\partial u}{\partial t} &= D_{u_x} \frac{\partial^2 u}{\partial x^2} + D_{u_y} \frac{\partial^2 u}{\partial y^2} - uv^2 + f(1 - u) & - D_{u_x} \text{ and } D_{u_y} \text{ are the diffusion rates for } u \text{ in the } x\text{- and } y\text{-directions.} \\ \frac{\partial v}{\partial t} &= D_{v_x} \frac{\partial^2 v}{\partial x^2} + D_{v_y} \frac{\partial^2 v}{\partial y^2} + uv^2 - (f + k)v & - D_{v_x} \text{ and } D_{v_y} \text{ are the diffusion rates for } v \text{ in the } x\text{- and } y\text{-directions.} \end{aligned}$$

All other terms remain the same as in the standard Gray-Scott model. This anisotropic modification allows for spatial variation in the diffusion dynamics, introducing a directional bias that can generate the stripe patterns required for the zebra pattern. As a result, the anisotropic Gray-Scott model successfully produces the desired pattern, as shown in Fig. 9.

Along with the other approaches discussed in Section 2, the expressivity bottleneck of the model exemplifies how our method can guide the search for mechanistic models. While the method can simply fail due to the optimization being challenging, by iteratively expanding a conjectured model until it achieves an expressivity level compatible with observed data, we can use the method to potentially identify missing mechanisms and refine our understanding of pattern formation in nature.

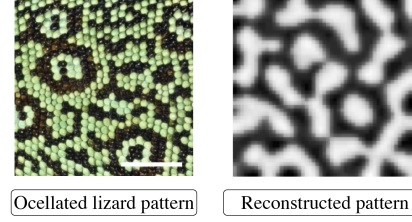


Figure 8: **Reconstruction of ocellated lizard pattern.** *Left:* Photograph of an ocellated lizard from Manukyan et al. [8], white bar indicates 5mm scale. *Right:* Reconstructed pattern by the set of reaction-diffusion parameters found by the method. Cosine similarity between target and reconstruction 0.773 ± 0.02 , for 100 evaluations.

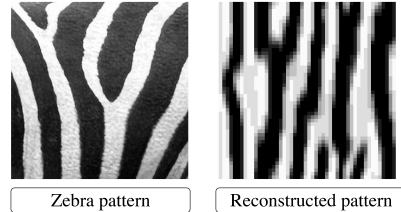


Figure 9: **Reconstruction of a zebra pattern.** *Left:* Photograph of a zebra skin pattern [55]. *Right:* Pattern generated by the anisotropic reaction-diffusion model for the parameters found by the method. Cosine similarity between target and reconstruction 0.842 ± 0.018 , for 100 evaluations.

5 Conclusion

In this work, we have presented a method for solving inverse problems in stochastic self-organizing systems by leveraging invariant visual representations from embedding models—without the need to handcraft metric functions to capture the visual similarities between patterns. The key idea is to shift the optimization from pixel space to an embedding space where perceptually similar patterns are mapped to nearby points, allowing the recovery of unknown parameters, even those resulting in stochastic patterns. Unlike existing techniques in inverse modeling, the method addresses the issue of stochasticity in the observable space, rather than in the causal space.

We have demonstrated the method on three distinct self-organizing systems spanning physics, biology and computational sociology: a reaction-diffusion system, a developmental model of embryogenesis, and an agent-based segregation model, all exhibiting stochasticity in the observation space. For the reaction-diffusion model, we have shown that the approach can be applied to real biological patterns: an ocellated lizard and a zebra skin pattern. Finally, we have illustrated how the framework can guide model testing: when a conjectured model fails to generate the target, it suggests that the model’s expressivity is insufficient and extra terms are needed, a practical path for iterative refinement in mechanistic modeling. In summary, the method provides a simple yet effective technique for theorists and experimentalists to investigate and control self-organizing stochastic systems.

5.1 Limitations

Embedding capturing the wrong invariances. The embedding representations are only useful to the extent that they are capable of encoding the invariances present in the target patterns. If the embedding model fails to capture the relevant features of the patterns—or encode non-relevant invariances—the optimization process may converge to parameters that reproduce visually dissimilar results, despite low embedding losses. For example, an embedding might prioritise shape over size, which can lead to false positives in parameter recovery. In other words, the embedding model is capturing an invariance, but might not be an invariance that we want. While this property may be desirable for certain problems, it can pose challenges for others. An example of this issue is illustrated in Fig. 10 where the technique finds a set of parameters that reproduce the target patterns but at a reduced scale.

5.2 Future Work

Domain-specific embedding models. One future direction is the use of custom embedding models trained specifically on the types of patterns relevant to the target domain. This could involve fine-tuning or training embedding models—e.g., a variational autoencoder trained on a domain-specific dataset [39]—or augmenting the dataset with relevant transformations for which we want the embedding model to be invariant. This way, the embedding space can be aligned more closely with the visual equivalence classes that matter for the task. Domain-specific embeddings could provide a way of ensuring that the method results in perceptually meaningful reconstructions.

Search on model space When solving an inverse problem, the search space can be the parameters of the forward model $\theta \in \Theta$, the functional form of the model F itself, or the initial configuration $s_0 \in S$ of the system. In this work, we have focused on only the first two cases. A future avenue will be to combine the method with modern symbolic regression techniques [54, 56] to recover the functional forms of the underlying models, and evaluate the method when searching in state space.

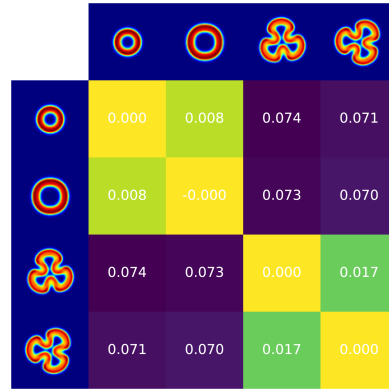


Figure 10: **Embedding invariances.** Distance matrix of four different patterns. CLIP model maps patterns with scale and rotation transformations to similar embedding vectors.

6 Acknowledgements

We thank Milton L. Montero for the discussion on the anisotropy of the reaction-diffusion model. This project was supported by the Novo Nordisk Foundation Synergy Grant *REPROGRAM* number NNF23OC0086722.

References

- [1] Thomas C. Schelling. Dynamic models of segregation. *Journal of Mathematical Sociology*, 1: 143–186, 1971. URL <https://api.semanticscholar.org/CorpusID:120637340>.
- [2] Federico Bianchi and Flaminio Squazzoni. Agent-based models in sociology. *WIREs Comput. Stat.*, 7(4):284–306, July 2015. ISSN 1939-5108. doi: 10.1002/wics.1356.
- [3] E. Samanidou, E. Zschischang, D. Stauffer, and T. Lux. Agent-based models of financial markets. *Rep. Prog. Phys.*, 70(3):409, February 2007. ISSN 0034-4885. doi: 10.1088/0034-4885/70/3/R03.
- [4] Adam J. McLane, Christina Semeniuk, Gregory J. McDermid, and Danielle J. Marceau. The role of agent-based models in wildlife ecology and management. *Ecol. Model.*, 222(8):1544–1556, April 2011. ISSN 0304-3800. doi: 10.1016/j.ecolmodel.2011.01.020.
- [5] Tatiana Filatova, Peter H. Verburg, Dawn Cassandra Parker, and Carol Ann Stannard. Spatial agent-based models for socio-ecological systems: Challenges and prospects. *Environ. Model. Software*, 45:1–7, July 2013. ISSN 1364-8152. doi: 10.1016/j.envsoft.2013.03.017.
- [6] Eric Bonabeau. From Classical Models of Morphogenesis to Agent-Based Models of Pattern Formation. *Artif. Life*, 3(3):191–211, July 1997. ISSN 1064-5462. doi: 10.1162/artl.1997.3.3.191.
- [7] Chad M. Glen, Melissa L. Kemp, and Eberhard O. Voit. Agent-based modeling of morphogenetic systems: Advantages and challenges. *PLoS Comput. Biol.*, 15(3):e1006577, March 2019. ISSN 1553-7358. doi: 10.1371/journal.pcbi.1006577.
- [8] Liana Manukyan, Sophie A. Montandon, Anamarija Fofonjka, Stanislav Smirnov, and Michel C. Milinkovitch. A living mesoscopic cellular automaton made of skin scales. *Nature*, 544: 173–179, April 2017. ISSN 1476-4687. doi: 10.1038/nature22031.
- [9] Albert Tarantola. *Inverse Problem Theory and Methods for Model Parameter Estimation*. Society for Industrial and Applied Mathematics, 2005. ISBN 978-0-89871-572-9 978-0-89871-792-1. doi: 10.1137/1.9780898717921. URL <http://epubs.siam.org/doi/book/10.1137/1.9780898717921>.
- [10] Mario Bunge. Inverse problems. *Foundations of Science*, 24(3):483–525, 2009. ISSN 1572-8471. doi: 10.1007/s10699-018-09577-1. URL <https://doi.org/10.1007/s10699-018-09577-1>.
- [11] Rick Durrett. Stochastic spatial models. *SIAM review*, 41(4):677–718, 1999.
- [12] James D Murray. *Mathematical biology: I. An introduction*, volume 17. Springer Science & Business Media, 2007.
- [13] Philip Ball. *Shapes: nature’s patterns: a tapestry in three parts*. OUP Oxford, 2009.
- [14] Hermann Haken. Synergetics: An approach to self-organization. *Self-organizing systems: The emergence of order*, pages 417–434, 1987.
- [15] Stuart A Kauffman. The origins of order: Self-organization and selection in evolution. In *Spin glasses and biology*, pages 61–100. World Scientific, 1992.
- [16] Maya Paczuski and Per Bak. Self-Organization of Complex Systems. *arXiv*, June 1999. doi: 10.48550/arXiv.cond-mat/9906077.

- [17] John Von Neumann, Arthur W Burks, et al. Theory of self-reproducing automata. *IEEE Transactions on Neural Networks*, 5(1):3–14, 1966.
- [18] Paul Weiss and A. C. Taylor. Reconstitution of complete organs from single-cell suspensions of chick embryos in advanced stages of differentiation. *Proc. Natl. Acad. Sci. U.S.A.*, 46(9): 1177–1185, September 1960. doi: 10.1073/pnas.46.9.1177.
- [19] Craig W Reynolds. Flocks, herds and schools: A distributed behavioral model. In *Proceedings of the 14th annual conference on Computer graphics and interactive techniques*, pages 25–34, 1987.
- [20] Charles W. Groetsch. *Inverse Problems in the Mathematical Sciences*. Vieweg+Teubner Verlag, Wiesbaden, Germany, 1993. ISBN 978-3-322-99202-4. URL <https://link.springer.com/book/10.1007/978-3-322-99202-4>.
- [21] Marko Vauhkonen, Tanja Tarvainen, and Timo Lähivaara. Inverse Problems. In *Mathematical Modelling*, pages 207–227. Springer, Cham, Switzerland, July 2016. ISBN 978-3-319-27836-0. doi: 10.1007/978-3-319-27836-0_12.
- [22] Nan Ye, Farbod Roosta-Khorasani, and Tiangang Cui. Optimization Methods for Inverse Problems. In *2017 MATRIX Annals*, pages 121–140. Springer, Cham, Switzerland, March 2019. ISBN 978-3-030-04161-8. doi: 10.1007/978-3-030-04161-8_9.
- [23] Housen Li, Johannes Schwab, Stephan Antholzer, and Markus Haltmeier. Nett: Solving inverse problems with deep neural networks. *Inverse Problems*, 36(6):065005, 2020.
- [24] Bahjat Kawar, Gregory Vaksman, and Michael Elad. Snips: Solving noisy inverse problems stochastically. *Advances in Neural Information Processing Systems*, 34:21757–21769, 2021.
- [25] Kailai Xu and Eric Darve. Solving inverse problems in stochastic models using deep neural networks and adversarial training. *Computer Methods in Applied Mechanics and Engineering*, 384:113976, 2021.
- [26] Martin Genzel, Jan Macdonald, and Maximilian März. Solving inverse problems with deep neural networks—robustness included? *IEEE transactions on pattern analysis and machine intelligence*, 45(1):1119–1134, 2022.
- [27] Andrea Frome, Greg S Corrado, Jon Shlens, Samy Bengio, Jeff Dean, Marc’ Aurelio Ranzato, and Tomas Mikolov. Devise: A deep visual-semantic embedding model. *Advances in neural information processing systems*, 26, 2013.
- [28] Mohammad Norouzi, Tomas Mikolov, Samy Bengio, Yoram Singer, Jonathon Shlens, Andrea Frome, Greg S Corrado, and Jeffrey Dean. Zero-shot learning by convex combination of semantic embeddings. *arXiv preprint arXiv:1312.5650*, 2013.
- [29] Chao Jia, Yinfei Yang, Ye Xia, Yi-Ting Chen, Zarana Parekh, Hieu Pham, Quoc V. Le, Yunhsuan Sung, Zhen Li, and Tom Duerig. Scaling Up Visual and Vision-Language Representation Learning With Noisy Text Supervision. *arXiv*, February 2021. doi: 10.48550/arXiv.2102.05918.
- [30] Eyvind Niklasson, Alexander Mordvintsev, Ettore Randazzo, and Michael Levin. Self-Organising Textures. *Distill*, 6(2):e00027.003, February 2021. ISSN 2476-0757. doi: 10.23915/distill.00027.003.
- [31] Yingtao Tian and David Ha. Modern Evolution Strategies for Creativity: Fitting Concrete Images and Abstract Concepts. *arXiv*, September 2021. doi: 10.48550/arXiv.2109.08857.
- [32] Olga Moskvyyak and Frederic Maire. Learning Geometric Equivalence between Patterns Using Embedding Neural Networks. In *2017 International Conference on Digital Image Computing: Techniques and Applications (DICTA)*, pages 2017–01. IEEE, 2017. doi: 10.1109/DICTA.2017.8227457.
- [33] Alec Radford, Jong Wook Kim, Chris Hallacy, Aditya Ramesh, Gabriel Goh, Sandhini Agarwal, Girish Sastry, Amanda Askell, Pamela Mishkin, Jack Clark, Gretchen Krueger, and Ilya Sutskever. Learning Transferable Visual Models From Natural Language Supervision. *arXiv*, February 2021. doi: 10.48550/arXiv.2103.00020.

- [34] Akarsh Kumar, Chris Lu, Louis Kirsch, Yujin Tang, Kenneth O. Stanley, Phillip Isola, and David Ha. Automating the Search for Artificial Life with Foundation Models. *arXiv*, December 2024. doi: 10.48550/arXiv.2412.17799.
- [35] Ian Goodfellow, Honglak Lee, Quoc Le, Andrew Saxe, and Andrew Ng. Measuring invariances in deep networks. *Advances in neural information processing systems*, 22, 2009.
- [36] Zhuotun Zhu, Xinggang Wang, Song Bai, Cong Yao, and Xiang Bai. Deep learning representation using autoencoder for 3d shape retrieval. *Neurocomputing*, 204:41–50, 2016.
- [37] Michael Tschannen, Olivier Bachem, and Mario Lucic. Recent advances in autoencoder-based representation learning. *arXiv preprint arXiv:1812.05069*, 2018.
- [38] Richard Zhang, Phillip Isola, Alexei A. Efros, Eli Shechtman, and Oliver Wang. The Unreasonable Effectiveness of Deep Features as a Perceptual Metric. *arXiv*, January 2018. doi: 10.48550/arXiv.1801.03924.
- [39] Maximilian Ilse, Jakub M Tomczak, Christos Louizos, and Max Welling. Diva: Domain invariant variational autoencoders. In *Medical Imaging with Deep Learning*, pages 322–348. PMLR, 2020.
- [40] N. Hansen and A. Ostermeier. Adapting arbitrary normal mutation distributions in evolution strategies: the covariance matrix adaptation. In *Proceedings of IEEE International Conference on Evolutionary Computation*, pages 312–317. IEEE, May 1996. ISBN 978-0-7803-2902. URL <https://ieeexplore.ieee.org/document/542381>.
- [41] Luis Miguel Rios and Nikolaos V. Sahinidis. Derivative-free optimization: a review of algorithms and comparison of software implementations. *J. Global Optim.*, 56(3):1247–1293, July 2013. ISSN 1573-2916. doi: 10.1007/s10898-012-9951-y.
- [42] Nacim Belkhir, Johann Dréo, Pierre Savéant, and Marc Schoenauer. Per instance algorithm configuration of CMA-ES with limited budget. In *ACM Conferences*, pages 681–688. Association for Computing Machinery, New York, NY, USA, July 2017. doi: 10.1145/3071178.3071343.
- [43] Konstantinos Varelas, Anne Auger, Dimo Brockhoff, Nikolaus Hansen, Ouassim Ait ElHara, Yann Semet, Rami Kassab, and Frédéric Barbaresco. A Comparative Study of Large-Scale Variants of CMA-ES. In *Parallel Problem Solving from Nature – PPSN XV*, pages 3–15. Springer, Cham, Switzerland, August 2018. ISBN 978-3-319-99253-2. doi: 10.1007/978-3-319-99253-2_1.
- [44] Keith C. Bledsoe, Jeffrey A. Favorite, and Tunc Aldemir. Application of the Differential Evolution Method to Solving Inverse Transport Problems. *Nucl. Sci. Eng.*, October 2011. ISSN 1184-1355. URL <https://www.tandfonline.com/doi/abs/10.13182/NSE10-28>.
- [45] Alexander V. Grayver and Alexey V. Kuvshinov. Exploring equivalence domain in nonlinear inverse problems using Covariance Matrix Adaption Evolution Strategy (CMAES) and random sampling. *Geophys. J. Int.*, 205(2):971–987, May 2016. ISSN 0956-540X. doi: 10.1093/gji/ggw063.
- [46] John E. Pearson. Complex Patterns in a Simple System. *Science*, 261(5118):189–192, July 1993. ISSN 0036-8075. doi: 10.1126/science.261.5118.189.
- [47] Kyoung J. Lee, W. D. McCormick, Qi Ouyang, and Harry L. Swinney. Pattern Formation by Interacting Chemical Fronts. *Science*, 261(5118):192–194, July 1993. ISSN 0036-8075. doi: 10.1126/science.261.5118.192.
- [48] Zixuan Cang, Yangyang Wang, Qixuan Wang, Ken WY Cho, William Holmes, and Qing Nie. A multiscale model via single-cell transcriptomics reveals robust patterning mechanisms during early mammalian embryo development. *PLoS computational biology*, 17(3):e1008571, 2021.
- [49] JD Biggers, JOAN E Bell, and DALE J Benos. Mammalian blastocyst: transport functions in a developing epithelium. *American Journal of Physiology-Cell Physiology*, 255(4):C419–C432, 1988.

- [50] Morpheus. Blastocyst Development | Morpheus. *Morpheus*, April 2025. URL <https://morpheus.gitlab.io/model/m9999>.
- [51] William AV Clark and Mark Fossett. Understanding the social context of the schelling segregation model. *Proceedings of the National Academy of Sciences*, 105(11):4109–4114, 2008.
- [52] Zach Nussbaum, Brandon Duderstadt, and Andriy Mulyar. Nomic Embed Vision: Expanding the Latent Space. *arXiv*, June 2024. doi: 10.48550/arXiv.2406.18587.
- [53] Lokesh Veeramacheneni, Moritz Wolter, Hildegard Kuehne, and Juergen Gall. Fréchet Wavelet Distance: A Domain-Agnostic Metric for Image Generation. *arXiv*, December 2023. doi: 10.48550/arXiv.2312.15289.
- [54] Miles Cranmer. Interpretable machine learning for science with pysr and symbolicregression. *arXiv preprint arXiv:2305.01582*, 2023.
- [55] Emmett Lindner. Last of Escaped Zebras Captured After Being Lured With White Bread. *N.Y. Times*, May 2024. ISSN 0362-4331. URL <https://www.nytimes.com/2024/05/04/us/zebra-washington-state-highway-captured.html>.
- [56] Silviu-Marian Udrescu and Max Tegmark. AI Feynman: A physics-inspired method for symbolic regression. *Sci. Adv.*, 6(16), April 2020. ISSN 2375-2548. doi: 10.1126/sciadv.aay2631.

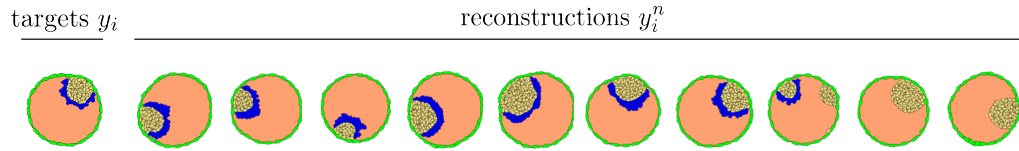


Figure 12: **Results for blastocyst embryonic developmental model.** A single target pattern y_i (*left column*), simulated based on a Cellular Potts model [50]. The developmental process is implemented as a set of stochastic differential equations [48, 50]. The reconstructions columns show the patterns y_i^n recovered by our method for 10 independent training runs. The corresponding training curves and loss histograms are shown in Figure 6.

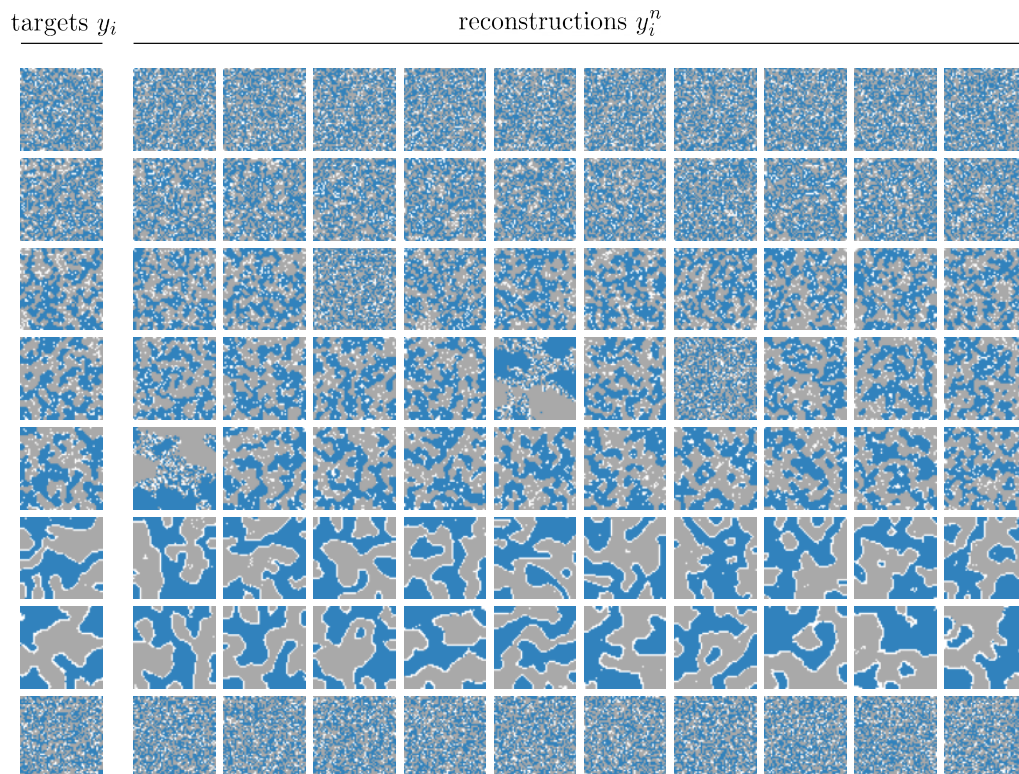


Figure 13: **Results for Schelling's segregation model.** Eight target patterns y_i (*left column*), each produced by simulating Schelling ABM model of segregation 4.3 for different parameters θ_i and random initial states s_{0i} . The reconstructions columns show the patterns y_i^n recovered by our method for 10 independent training runs. The corresponding training curves and loss histograms are shown in Figure 7.

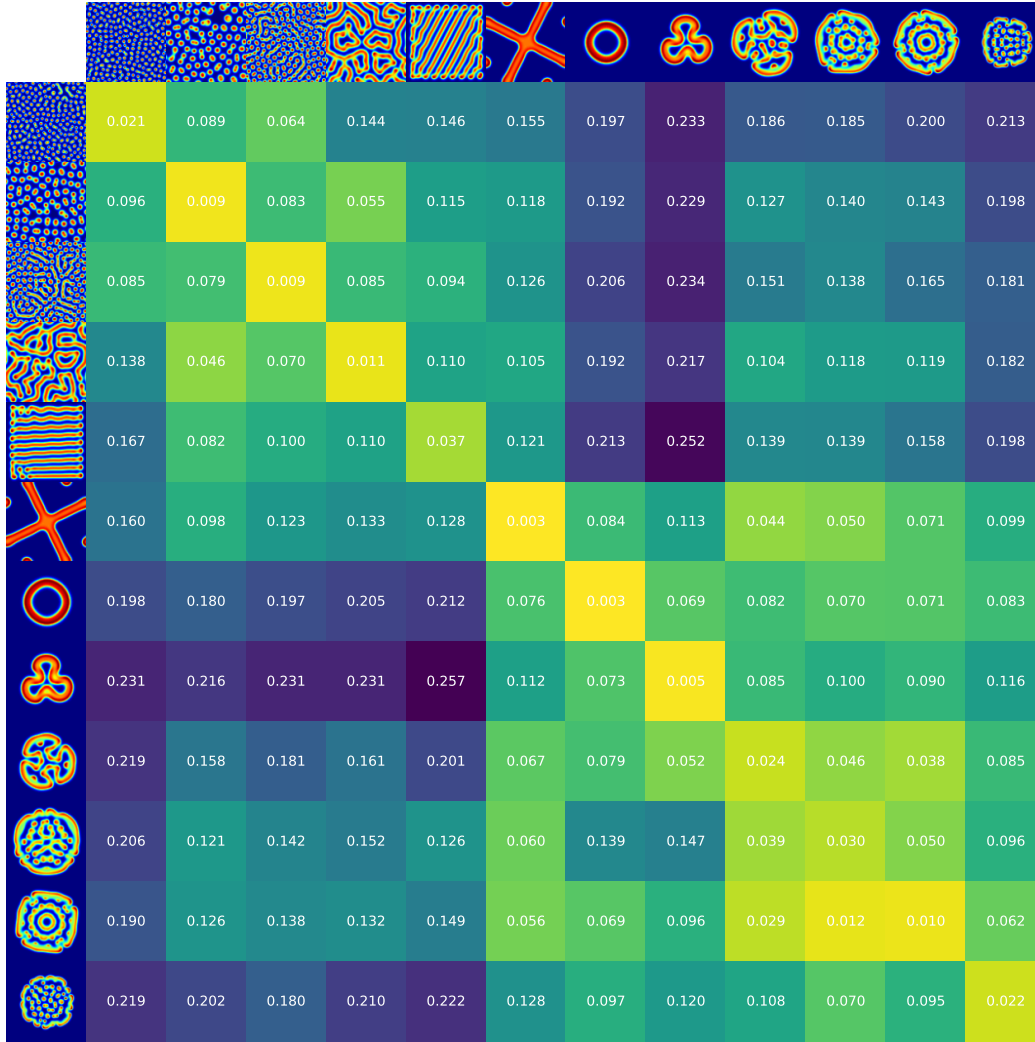


Figure 14: **Embedding invariance across pattern instances of Gray-Scott model.** Cosine distance matrix between CLIP embeddings of two sets of 12 patterns, Y and Y' . Each set of patterns is generated using the same set of parameters $\theta_i \in \Theta$ and a sampled initial configuration $s_0 \sim \mathcal{S}$. The inner matrix displays the pairwise cosine distances $1 - \cos(z_i, z'_i)$ between the embeddings z_i and z'_i of patterns $y_i \in Y$ and $y'_i \in Y'$. The advantage of the invariant representation is evident in the high similarity (i.e., low cosine distance) along the diagonal, indicating that different pattern instances generated from the same causal parameter $\theta \in \Theta$ but different initial configuration $s_{0i} \sim \mathcal{S}$ are represented closely together in embedding space.



Figure 15: Embedding invariance across pattern instances of blastocyst model. Distance matrix between two different sets of 5 blastocyst patterns at different stages of development, Y and Y' under CLIP metric. Each pair of patterns at a given developmental stage is generated using the same set of causal parameters Θ and different stochastic initial states S . The inner matrix displays the pairwise cosine distances $1 - \cos(z_i, z'_i)$ between the embeddings z_i and z'_i of patterns $y_i \in Y$ and $y'_i \in Y'$. Unlike reaction-diffusion and Schelling's segregation model, the blastocyst has a single ground-truth pattern as seen during mammal embryonic development. Hence, to illustrate how CLIP embedding captures similarities, we demonstrate embedding similarity for different developmental stages.

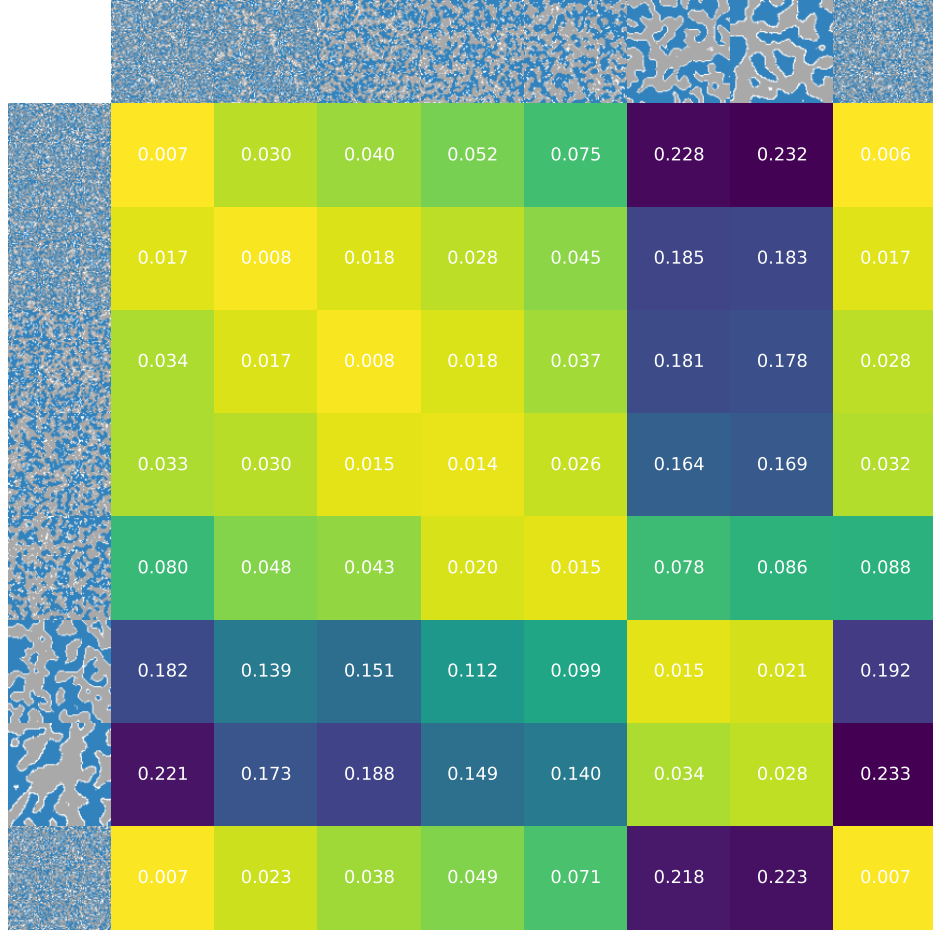


Figure 16: **Embedding invariance across pattern instances of Schelling’s model.** Distance matrix between two different sets of 8 patterns, Y and Y' under CLIP metric. Each set of patterns is generated using the same set of causal parameters Θ and different stochastic initial states \tilde{S} under the Schelling model. The inner matrix displays the pairwise cosine distances $1 - \cos(z_i, z'_i)$ between the embeddings z_i and z'_i of patterns $y_i \in Y$ and $y'_i \in Y'$. As described in Fig. 7, Schelling’s model is non-injective and produces similar patterns y_i and y'_i for certain parameters, such as $\theta = T = 0.1$ and $\theta' = T' = 0.8$, a property reflected in both the observable space and the embedding distances.